Simple relative space-time scaling of electrical and electromagnetic depth sounding arrays: Implications for electrical static shift removal and joint DC-TEM data inversion with th...

1 AUTHOR:

Max A. Meju
PETRONAS

71 PUBLICATIONS **1,334** CITATIONS

Simple relative space–time scaling of electrical and electromagnetic depth sounding arrays: implications for electrical static shift removal and joint DC-TEM data inversion with the most-squares criterion

Max A. Meju*

Department of Environmental Science, Lancaster University, Lancaster LA1 4YQ, UK

ABSTRACT

A simple scaling relationship is shown to facilitate comparison, correlation and integration of data recorded using the common experimental configurations in electrical and electromagnetic depth sounding. Applications of the scheme to field data from typical geological and landfill environments show that it is robust and, where transient electromagnetic (TEM) data are available, enables easy identification and quantification of electrical static shift (galvanic distortion) in magnetotelluric and direct current (DC) sounding curves. TEM-based procedures are suggested for both the direct removal of static shift in DC sounding curves and effective joint data inversion with the most-squares criterion in the presence of static shift. A case study of aquifer characterization using sounding data from borehole sites in the Vale of York in England shows that static shift is a common problem in this glacial-covered terrain and demonstrates the effectiveness of the proposed joint DC-TEM inversion strategy in handling distorted soundings.

INTRODUCTION AND PROBLEM DEFINITION

Several experimental configurations are used for electrical conductivity depth sounding (see, e.g., Morrison *et al*. 1996; Sørensen 1996, 1997; Panissod *et al*. 1998; Meju 2002, fig. 1). The recorded data bear the conductivity signature of the subsurface and allow conclusions to be drawn about the structure and sometimes the physiochemical state of geological and man-made targets (e.g. Chen *et al*. 1996; Morrison *et al*. 1996; Meju *et al*. 1999; Hautot *et al*. 2000; Meju 2000, 2002; Bai, Meju and Liao 2001). However, owing to technical limitations, no single conductivity depth-sounding technique provides complete, consistent and sufficient data to characterize the subsurface fully, and the effectiveness of each technique varies from one geological environment to another. The various measurements are influenced differently by the presence of small-sized three-dimensional (3D) bodies in the near-surface.

The identification and accurate removal of spurious near-surface 3D effects or geological noise in discrete (or single-station) depth soundings are still unresolved problems in geoelectrical exploration (see Berdichevsky and Dmitriev 1976; Barker 1981; Park 1985; Sternberg, Washburne and Pellerin 1988; Bahr 1988, 1991; Groom and Bailey 1989; Pellerin and Hohmann 1990; Groom and Bahr 1992; Spitzer 2001). Moreover, there is still the problem of integrating the numerous methods to obtain a consistent form of data presentation (Spies and Eggers 1986; Hobbs 1992; Das 1997; Meju 2002), making it sometimes difficult for the uninitiated to appreciate the complementary nature of the various techniques. The integration of electrical and electromagnetic data can improve the robustness of model interpretation and the cumulative probability of detection of subsurface targets.

Correlation, comparison or integration of data from the various electrical and electromagnetic (EM) sounding techniques is a non-trivial task. For example, in the direct current (DC) resistivity method where depth sounding is achieved by varying the electrode separations, the experimental data are shown as apparent resistivity versus electrode separation.

*E-mail: m.meju@lancaster.ac.uk

In the time-domain or transient electromagnetic (TDEM or TEM) method, where EM energy is applied to the ground by artificial transient pulses and multispectral measurements enable information to be obtained from different depths, the data are presented as apparent resistivity versus transient time (usually in ms) or the square-root of time in the Russian literature (Spies 1983). In the magnetotelluric (MT) method employing natural and/or artificial EM field variations on the surface to probe the subsurface, the measured apparent-resistivity data are presented as a function of frequency (or its reciprocal, period) and as apparent resistivity versus the square-root of period in the Russian literature (Spies 1983). There is no simple generalized scheme for comparing these depth-sounding arrays, and the non-specialist end-user sometimes views the experimental data obtained by these methods as disparate data sets constituting different 'data spaces'. It is highly desirable to eliminate subjectivity and achieve comparability between the various techniques in a general geological medium.

The aims of this paper are therefore: (i) to provide a simple consistent framework that brings together various ideas about the correspondence between electrical and EM data and their presentation methodology; (ii) to demonstrate the usefulness of this unified approach for assessing the consistency, completeness and sufficiency of field data and hence their suitability for combined interpretation; and (iii) to provide a data-consistent approach to joint inversion of electrical and EM data. As a starting point, a simple generic scaling relationship will be suggested for the electrode and coil configurations commonly used in conductivity depth sounding. This may serve for easy comparison of apparent-resistivity data, especially in experimental design and data quality control processes and, hopefully, will enable the derivation of more complete and consistent conductivity response profiles of the subsurface. The implications for static-shift identification (Bahr 1991; Spitzer 2001) and for effective joint inversion of field data from multiple methods are then examined using field data from different geological and man-made environments. Finally, an instructive case study of aquifer characterization is presented. It highlights the necessity for a combined analysis of TEM and electrical resistivity soundings in regions with glacial cover.

SCALING RELATIONSHIPS FOR TEMPORAL AND SPATIAL SOUNDING CONFIGURATIONS

It has been determined empirically (from numerical modelling and field studies of collocated DC resistivity and TEM depth soundings in different environments) that apparent-resistivity data from transient electromagnetic and steady-state electrical soundings with the popular symmetric in-line 4-electrode (Schlumberger, Wenner and dipole-dipole) arrays may be compared using the relationship,

$$t = 0.5\pi\mu\sigma L^2, \tag{1}$$

or equivalently, $L = 711.8\sqrt{t\rho}$ metres, where the transient time t is in seconds, μ is the magnetic permeability (taken to be equal to that of free-space: $\mu_0 = 4\pi \times 10^{-7}$ Ωs/m), L is one-half the electrode-array length (i.e. the distance from the centre of the array to an outermost electrode), and $\rho\ (= 1/\sigma)$ is the homogeneous subsurface resistivity (in Ωm), which is only known after data inversion and is hence conveniently approximated here by the apparent resistivity ρ_a (note that the all-time ρ_a is preferred in the TEM case). Since it has been shown semi-analytically and empirically that the equivalent MT period (T) for a given transient time in seconds is $T \cong 4t$ (see Sternberg *et al.* 1988; Meju 1998), we may then use (1) to define the scaling relationship for MT and DC resistivity as

$$T = 2\pi\mu\sigma L^2, \tag{2}$$

or $L = 355.9\sqrt{T\rho}$ metres. It follows that for given depth-sounding data (apparent resistivity versus time or frequency) from time-domain or frequency-domain EM experiments, we may estimate the half-electrode-array length for the appropriate in-line 4-electrode configuration that will yield the equivalent relative information and vice versa, making for a consistent presentation or easy comparison. Note that TEM and MT responses may show overshoot or undershoot effects near boundaries, i.e. the apparent-resistivity data are influenced by a 'bump' up or down on the sounding curve before a resistivity decrease or increase, respectively, which could hinder a direct comparison between the different types of data. However, this can be recognized in the relevant segments of the sounding curve and the problem may also be overcome by the use of an appropriate apparent-resistivity definition for TEM (e.g. Christensen 1995) or MT (e.g. Başokur 1994) when comparing the results with DC resistivity data, and by use of phase-corrected or effective resistivity transforms (see Meju 1998, eqn 1) when integrating with DC resistivity models.

In a previous attempt to relate TEM and DC resistivity soundings, Meju *et al.* (1999) proposed the scaling relationship $\log_{10}t \cong 2\log_{10}(L) - 5$ with t in ms, and used it to compare Schlumberger DC resistivity and TEM soundings in an area where the near-surface sedimentary rocks have average

resistivities of $100-200$ Ωm. If t is in ms (1) can be written (see Meju 2002, eqn 1) as

$$\log_{10} t = 2\log_{10}(L) - \log_{10}(2\rho/(10^3 \pi \mu)), \tag{3}$$

and it is easy to see that the relationship used by Meju *et al*. (1999) would only work in a specific environment since ρ varies in general. The present scheme eliminates subjectivity and achieves comparability in a general medium as demonstrated below.

EXAMPLES OF COMPATIBLE DATA PRESENTATIONS FOR COMPLETENESS, CONSISTENCY AND SUFFICIENCY ANALYSIS

The theoretical DC resistivity, TEM and MT apparent-resistivity responses of a hypothetical earth model, consisting of a succession of layers of different resistivities ($\rho_1 = 488$ Ωm, $\rho_2 = 110$ Ωm, $\rho_3 = 35$ Ωm, $\rho_4 = 73$ Ωm, $\rho_5 = 182$ Ωm, $\rho_6 = 45$ Ωm) and thicknesses ($h_1 = 1.96$ m, $h_2 = 7.2$ m, $h_3 = 23$ m, $h_4 = 38$ m, $h_5 = 122.7$ m, $h_6 = \infty$), are shown as functions of electrode spacing in Fig. 1(a) and of transient times in Fig. 1(b) using (1) and (2). The transmitter turn-off effect (Raiche 1984) was accounted for in the TEM calculations. A feature of this model is the presence of a conductor-confined stack of layers characterized by increasing resistivity with depth (layers 3, 4 and 5) that may be difficult to resolve using only EM apparent-resistivity data. Note that all the methods show concordant response patterns, with the DC resistivity technique being more sensitive to the deep resistive layer (182 Ωm) as is well known (this feature can be used to recognize, at first glance, the presence of more than one resistive stratigraphic unit sandwiched between two conductive layers in the subsurface); the EM methods will be more sensitive to good conductors, hence the need for an integrated approach in subsurface investigations.

Figure 2(a,b) shows examples of relative space–time scaling and the comparability of DC resistivity and TEM data for soundings over granular aquiferous deposits in the Netherlands (Meekes and van Will 1991) and over an old landfill site at Leighton Buzzard in England. Note that there is a good match between the transformed data for a given technique and the actual observed data for the other method. A very conductive basal substratum is sensed by both the TEM data from the Netherlands (see Meekes and van Will 1991) and the landfill site, but the complementary DC resistivity data suggest the presence of a sequence of geoelectrical units of increasing resistivity directly on top of the basal conduc-

tor. This is a situation analogous to the hypothetical model response shown in Fig. 1(a,b). However, compared with the scenario depicted in Fig. 1, these DC and TEM field data sets appear somewhat band-limited and may therefore be insufficient for accurately characterizing the basal section at the respective sounding sites.

The proposed scaling relationships can be applied to bidirectional DC and MT soundings with electrode arrays deployed in consistent orthogonal geographical directions in heterogeneous geological media, where the resistivity varies not only with depth but also laterally. Figure 3(a) shows Schlumberger DC, central-loop TEM and bi-directional MT apparent-resistivity data from the same sounding station in the Parnaiba Basin in NE Brazil (Meju *et al*. 1999). All the data are presented as a function of MT frequency. It is clear that all the methods give concordant sounding curves. The same concordant curves are revealed when the data are presented as a function of period or the equivalent electrode separation, using the suggested scaling relationships. This is an example of a relatively complete, sufficient and consistent data set for imaging the resistivity distribution in the top 2 km beneath the station. Figure 3(b) shows the Schlumberger DC and MT apparent-resistivity data for bi-directional soundings with the electric dipoles oriented across strike (north–south) and along strike (east–west) of a subcropping heavily fractured granodiorite basement (Meju, Gallardo and Mohamed 2003). The DC soundings employed half-current-electrode spacings (*AB*/2) of 1.5–90 m. The combined natural and controlled source MT recordings (with the Geometrics STRATAGEM Model EH4 equipment) are taken over a frequency range of 10–89 000 Hz. The data from collocated central-loop TEM soundings are also shown for comparison. The apparent-resistivity curves for each sounding direction are very similar and are shown as a function of DC electrode spacing. It is obvious that the suggested scaling relationships for data presentation apply in the general geological medium.

IDENTIFICATION OF ELECTRICAL STATIC SHIFT IN MT AND DC SOUNDINGS

It is well known that the presence of small-scale heterogeneities near the ground surface at a sounding position will cause MT and DC resistivity sounding curves to be distorted or biased (e.g. Barker 1981; Bahr 1991; Spitzer 2001) and, if unaccounted for, will lead to erroneous interpretations. However, accurate removal of this galvanic distortion or 'electrical static shift' in discrete field sounding curves is still an unresolved problem. In cases where only DC resistivity and MT
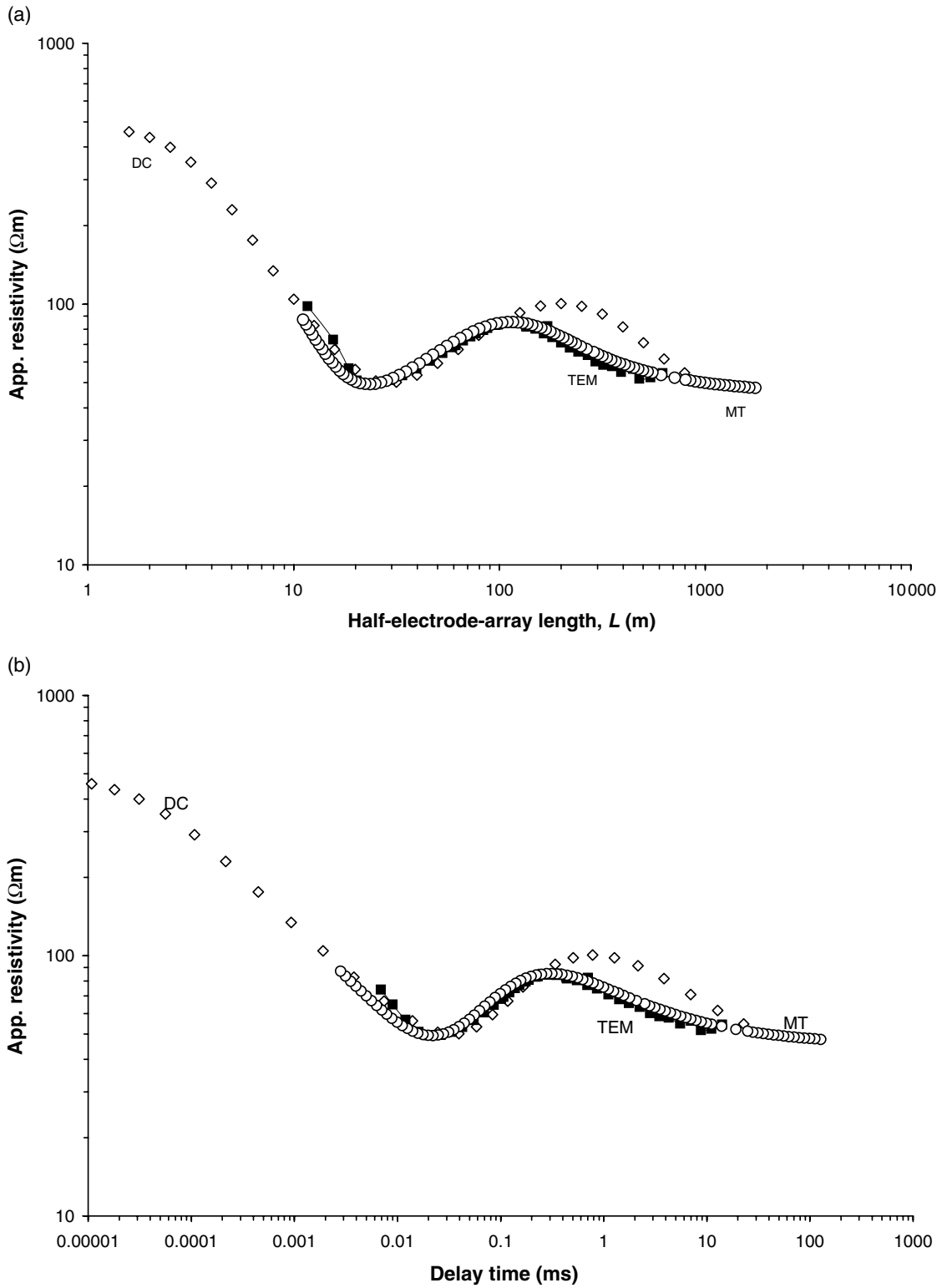
(a)

(b)

Figure 1 Equivalent presentation of synthetic electrical and EM responses for a 6-layer model. The Schlumberger DC resistivity (*AB*/2 spacings of 1–800 m) (◇), TEM (0.007–30 ms) (■) and MT (1–89 125 Hz) (○) data are presented as functions of (a) half the electrode-array length and (b) transient times, using the proposed scaling relationships.
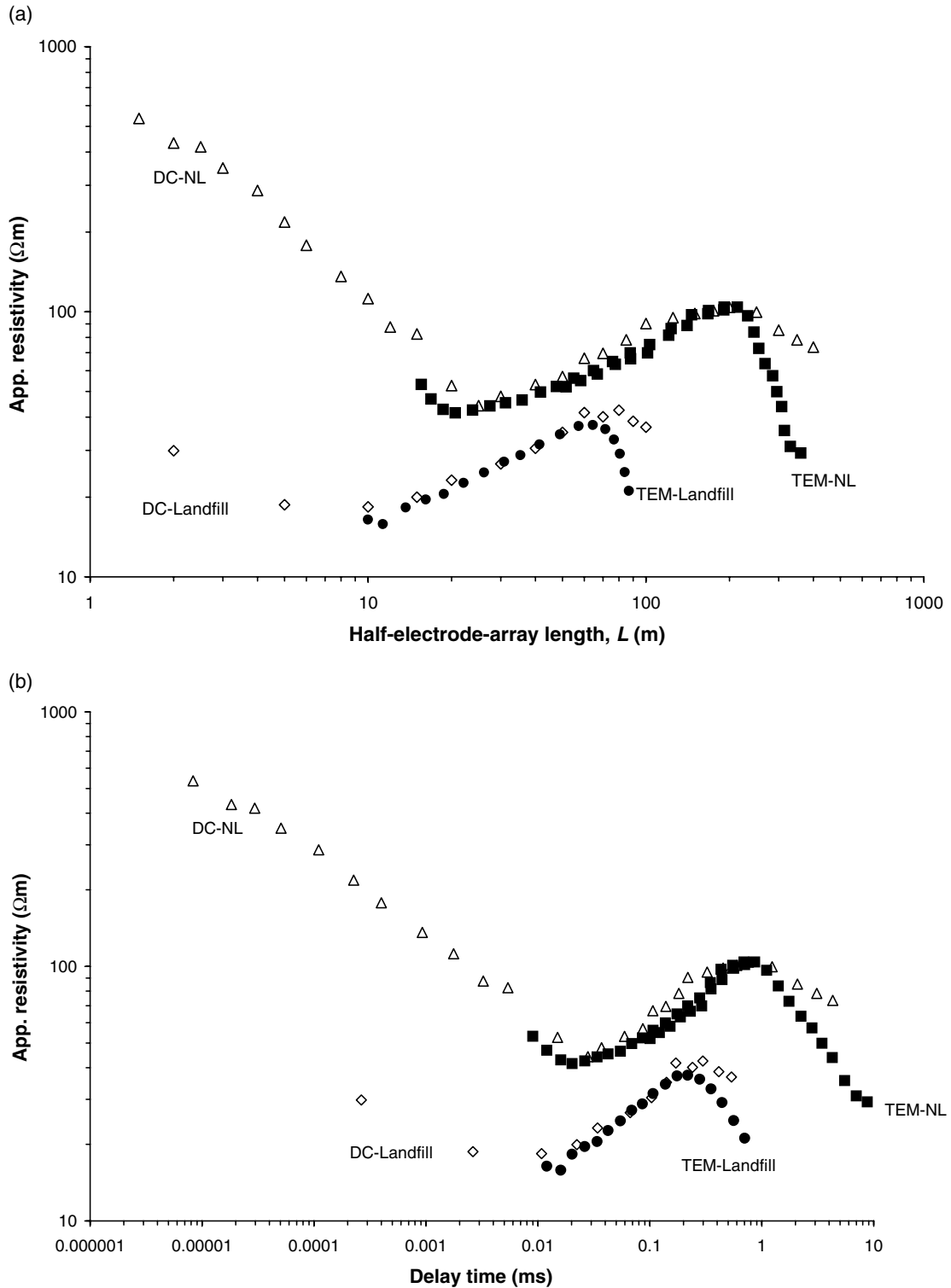
(a)

(b)

Figure 2 Equivalent presentation of Schlumberger DC resistivity and TEM sounding data from natural and man-made environments. (a) The data are presented as a function of half the electrode-array length. (b) The data are presented as a function of transient time. The acronym NL denotes data from the Netherlands (Meekes and van Will 1991), Landfill denotes data from an old covered landfill site in the UK. △, DC-NL; ■, TEM-NL; ◇, DC-Landfill; ●, TEM-Landfill.
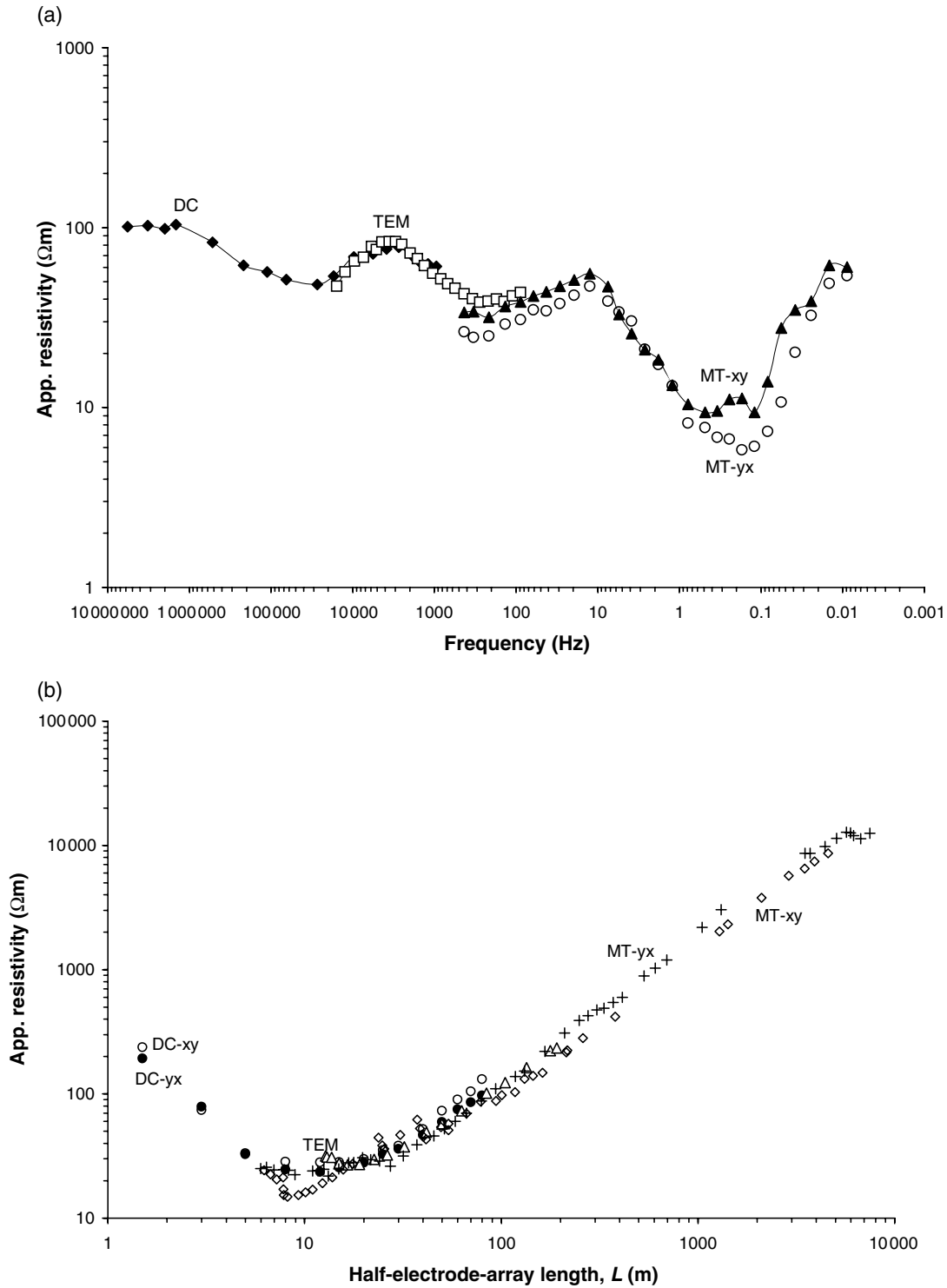
Figure 3 Examples of relative space–time scaling of TEM and bi-directional DC and MT field data to yield broadband integrated soundings. (a) Schlumberger DC resistivity, central-loop TEM and MT soundings at a deep borehole site in the Parnaiba Basin, Brazil (Meju *et al*. 1999). The DC sounding position is offset 40 m from the TEM and MT sounding point. ♦, DC; □, TEM; ▲, MT-xy; ○, MT-yx. (b) Collocated Schlumberger DC, central-loop TEM and CSMT soundings over a granodiorite batholith in the English Midlands (Meju *et al*. 2003). ○, DC-xy; ●, DC-yx; ◇, MT-xy; +, MT-yx; △, TEM. In both plots, xy and yx denote north–south and east–west sounding directions, respectively.
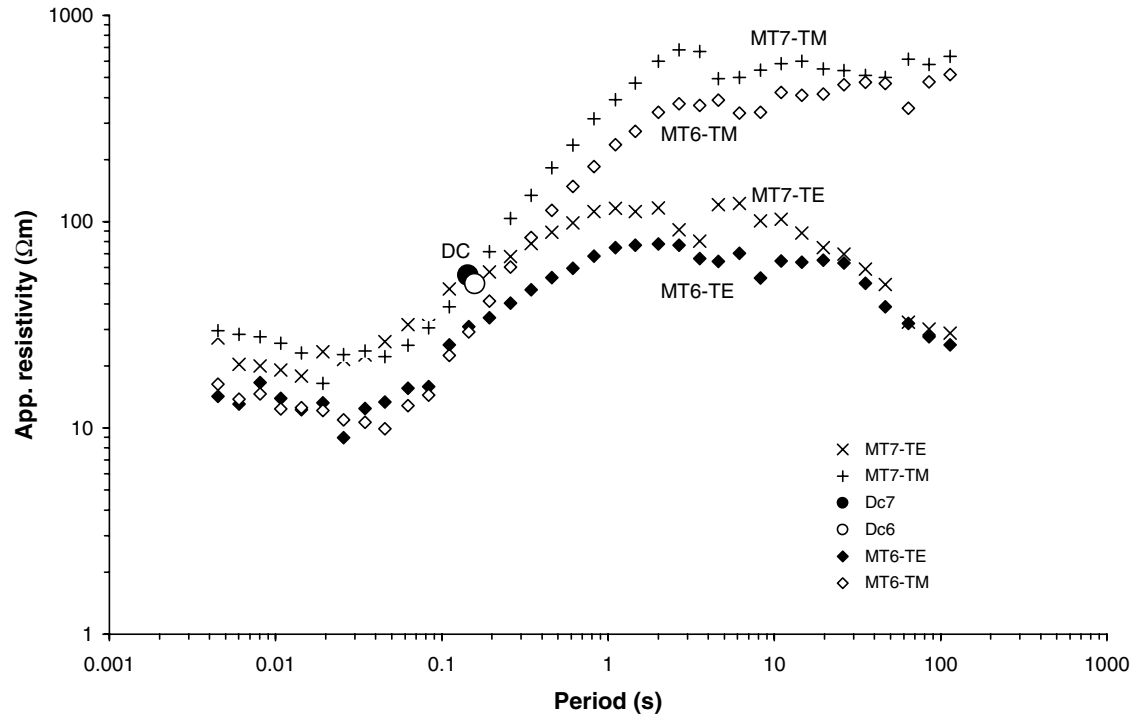
Figure 4 Comparative analysis of dual-mode MT sounding curves and single-spacing Schlumberger apparent-resistivity data (*AB*/2 = 1000 m) at two locations in the Ruili Basin in China (Bai and Meju 2003). The MT6 sounding curves appear to be affected by static shift.

data are available (e.g. Bai and Meju 2003), (2) would allow the direct use of DC resistivity data for assessing the static shift in MT data, but only in field situations where the DC soundings are not themselves affected by the same surficial heterogeneities that caused the MT static shift. It may thus be preferable to use non-coincident DC soundings for MT static shift analysis. To illustrate this, Fig. 4 shows the MT dual-polarization apparent-resistivity curves at two locations, 1 km apart, in the Ruili Basin in southeast China (Bai and Meju 2003). The DC apparent-resistivity data from reconnaissance profiling near the MT sites using the Schlumberger array with a half-current-electrode spacing (*AB*/2) of 1000 m (Liao and Zhao 1999, pp. 130–132) are also shown in Fig. 4 for comparison. The relative MT period for this electrode spacing was determined using (2). Note that one set of the dual-polarization MT sounding curves (MT6) appears to be affected significantly by static shift when compared with the DC data; the same deduction was arrived at by Bai and Meju (2003) when examining the result of tensor decomposition of the MT data (Groom and Bailey 1989; Bahr 1991).

Where TEM data are available, (1) and (2) can aid simple identification of MT or DC apparent-resistivity sounding curves affected by static shift in heterogeneous media. The use

of TEM to correct static shifts in MT soundings is well established (e.g. Sternberg *et al*. 1988; Meju 1996; Meju *et al*. 1999, 2003; Mohamed, Meju and Fontes 2002; Sakkas *et al*. 2002). However, the identification and accurate removal of static effects in DC resistivity and IP sounding curves (see Lee and Swartz 1930; Habberjam and Watkins 1976; Barker 1981) using TEM data has not received any attention in the literature, even though static shift is a galvanic effect that affects both MT and electrical resistivity soundings (see Pellerin and Hohmann 1990; Spitzer 2001). Various techniques have been proposed for combined 1D analysis of seemingly disparate DC and TEM data but these do not deal with the specific issue of static-shift identification and removal in DC soundings using TEM constraints. These techniques range from those incorporating the coefficient of layer anisotropy in joint inversion (e.g. Christensen 2000) to those involving mutually constrained inversion with no necessity for the coefficient of anisotropy (Auken, Pellerin and Sørensen 2001). A unified data-consistent approach is sought in this paper.

Figure 5 shows the Schlumberger DC resistivity sounding curves for two orthogonal directions at a test station underlain by thick glacial deposits in Leicester, England. The bidirectional DC soundings are practically the same and, in
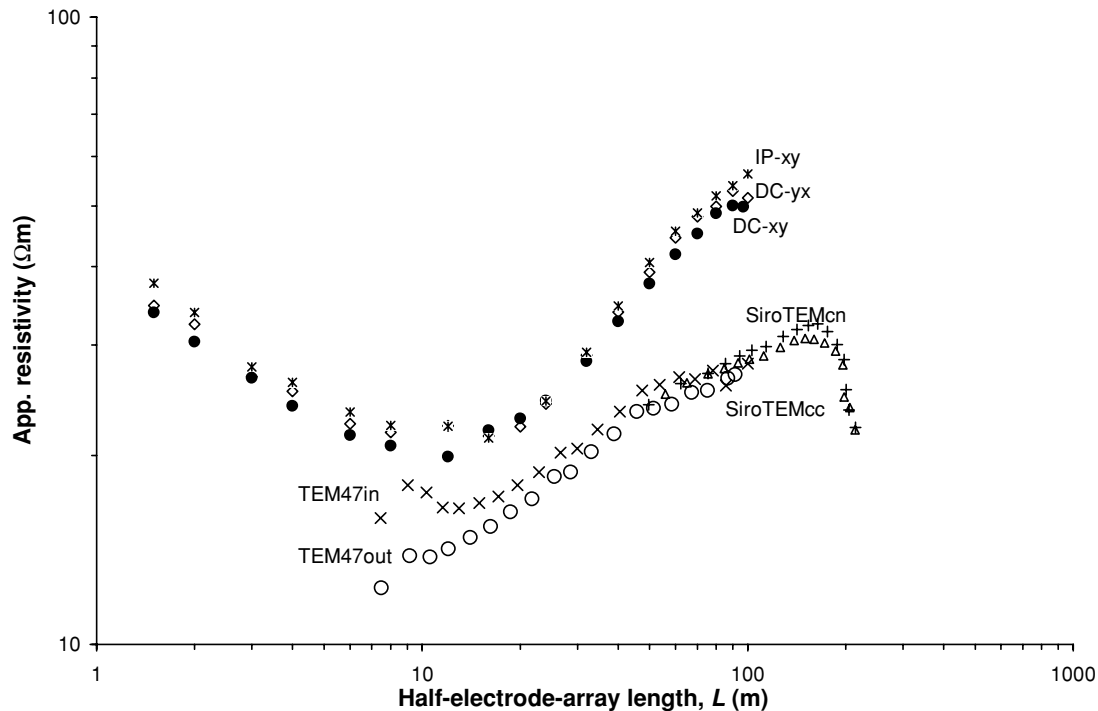
Figure 5 Bi-directional electrical (DC and IP) resistivity and multiple geometry TEM soundings at a glacial-covered test site in Leicester, England. The symbols xy and yx denote north–south and east–west electrical soundings, respectively. The TEM soundings employed a loop size of 100 m × 100 m (with the SiroTEM equipment) and 50 m × 50 m (with the Geonics TEM47 equipment). TEM47in (×) denotes a sounding with the data logger/control unit and operator located inside the transmitter loop (about 5 m away from the central dipole receiver). TEM47out (○) denotes a sounding with the data logger/control unit placed outside the transmitter loop. SiroTEMcn (+) and SiroTEMcc (△), respectively, denote central- and coincident-loop soundings. ●, DC-xy; ◇, DC-yx; ✳, IP-xy.

traditional exploration, would give the impression that uniform ground conditions exist at this site. The Wenner bi-directional sounding curves (not shown here) are identical to the Schlumberger curves. Collocated dipole-dipole array sounding with the IP method also yielded identical apparent-resistivity curves (see Fig. 5). The central-loop and single-loop TEM sounding curves from this site are also shown in Fig. 5 for comparison. Note that in central-loop soundings with the Geonics TEM47 field equipment (and transmitter loops with sides ≥ 40 m), it is routine practice for the data logger/control unit and operator to be located inside the transmitter loop, about 5 m away from the central dipole receiver (see curve marked 'TEM47in' in Fig. 5). At this site, the central-loop soundings were carried out with the data logger and system control unit placed outside the transmitter loop (see curve marked 'TEM47out' in Fig. 5). This was found to provide a partial remedy to the system-specific band-limitation problem facing TEM measurements as discussed by Effersø, Auken and Sørensen (1999). The relevant TEM soundings with different receiver–transmitter configurations and loop sizes (sides of

50 m and 100 m) at the Leicester site are in accord and would support the hypothesis that the deep subsurface is somewhat one dimensional. However, the observed electrical resistivity curves are displaced vertically by a significant amount from the overlapping TEM data, suggesting the possibility of electrical static shift at this site. The distorting influence of a 3D surficial patch in a stratified medium has been shown by Spitzer (2001) using a 3D numerical modelling approach. The critical issue for soundings in stratified environments is: How can we correct a static-shifted DC sounding curve to its undistorted level, assuming that the whole sounding curve is affected by a constant amount?

REMOVAL OF ELECTRICAL STATIC SHIFT AND THE IMPLICATION FOR EFFECTIVE JOINT DC-TEM INVERSION

The relationship between the observed static-shifted DC apparent resistivities (d_s), the correct apparent resistivities (d_r),

and the constant multiplicative static shift or site gain factor (g) at a sounding point may be written as

$$\mathbf{d}_s = g\mathbf{d}_r. \tag{4}$$

Accurate data interpretation requires knowledge of g. It was not possible to find a satisfactory and geologically meaningful joint 1D model for the Leicester DC and TEM apparent-resistivity curves (Fig. 5) using conventional joint inversion methods (e.g. Jupp and Vozoff 1977; Raiche *et al.* 1985; Meju 1996) without first correcting the affected DC data or accounting for the magnitude of the shift g in the joint inversion process as described below.

DC curve shifting approach

Essentially, the vertically shifted but parallel DC sounding curves (in the log domain) are made to match the overlapping TEM sounding curves at slowly varying or near-invariant curve segments, but there may be uncertainty as to whether the two curves actually coincide within the given sounding bandwidth. Where there is a great deal of overlap between the DC and large-loop TEM data, it is possible to invert the TEM data first and then correct the DC field curve using the predicted DC response of the optimal TEM model. However, the preferred curve correction approach is to find, by trial and error, an acceptable scaling factor (g) such that the corrected DC sounding curve ($\mathbf{d}_s/g$) yields a direct resistivity-versus-depth transformation (Meju 1995) that matches the transformation obtained by TEM (Meju 1998). The latter approach can be automated as described in the next section.

Joint DC-TEM inversion using a combined direct and iterative approach

In the preferred joint inversion approach, the DC and TEM sounding curves are first compared using (1) and an initial guess is made of the amount and direction of static shift. The interpretation problem is then posed as: Given a finite collection of noisy field sounding data, an initial estimate of the unknown static-shift factor (g_a) and the corresponding resistivity-versus-depth estimates from direct data transformation (Meju 1995, 1998) or available *a priori* information ($\mathbf{h}$), find, amongst all possible solutions on account of the data uncertainties, the correct value of g and hence a model ($\mathbf{m}$) that satisfies the observed data ($\mathbf{d}_s$ and $\mathbf{d}_t$) within a specified χ^2 misfit (q_0) and that also retains the key features of $\mathbf{h}$. The equivalent mathematical statement is:

minimize

$$U_1 = \frac{1}{\mu}(Q_1 + Q_2 - q_0) + Q_3, \tag{5}$$

where $Q_1 = \|\mathbf{W}_r\mathbf{d}_s - \mathbf{W}_r[gf_r(\mathbf{m})]\|^2$, $Q_2 = \|\mathbf{W}_t\mathbf{d}_t - \mathbf{W}_tf_t(\mathbf{m})\|^2$ and $Q_3 = \|\mathbf{Dm} - \mathbf{h}\|^2$. Here, $\mathbf{d}_t$ denotes the TEM apparent-resistivity field data, $f_r(\mathbf{m})$ and $f_t(\mathbf{m})$ denote the respective DC and TEM forward functionals, and $1/\mu$ is an undetermined multiplier. The diagonal weighting matrices $\mathbf{W}_r$ and $\mathbf{W}_t$ contain the reciprocals of the standard DC and TEM observational errors, respectively, and $\mathbf{D}$ may be a first-difference operator or the identity matrix.

Note that there are two targets in the above problem definition, i.e. the determination of the correct g, and the search for a specific joint model with $\chi^2 = q_0$. An equivalent and effective two-stage strategy is instead to minimize the expression,

$$U_2 = \frac{1}{\mu}(Q_1 + Q_2) + Q_3, \tag{6}$$

to determine the correct or best value of g, and then keeping this value and the corresponding $\mathbf{h}$ (which may incorporate any available *a priori* information from well logs) constant, use the iterative most-squares technique (Meju 1994) to satisfy the χ^2 condition specified in U_1. In other words, knowing $\mathbf{m}$ (the optimal least-squares model with $\chi^2 = q_{LS}$) and g, we seek the specific model $\mathbf{m}_{q0}$ that fits our data to the prescribed misfit (q_0), as the solution to the second-stage problem,

minimize

$$U_3 = \mathbf{m}^T\mathbf{b} + \frac{1}{2\mu}\{(Q_1 + Q_2 - q_0) + Q_3\}, \tag{7}$$

where each element of the joint projection vector $\mathbf{b}$ has a value of unity and $1/2\mu$ is a Lagrange multiplier.

For notational simplicity, if we define the quantities

$$\mathbf{W}_* = \begin{bmatrix} W_r & 0 \\ 0 & W_t \end{bmatrix}, \quad \mathbf{d}_* = \begin{bmatrix} \mathbf{d}_s \\ \mathbf{d}_t \end{bmatrix} \quad \text{and} \quad f_*(m) = \begin{bmatrix} gf_r(m) \\ f_t(m) \end{bmatrix},$$

the solution that minimizes U_1 or U_2 is given by

$$\mathbf{m} = [(\mathbf{W}_*\mathbf{A}_*)^T(\mathbf{W}_*\mathbf{A}_*) + \mu D^T D]^{-1}[(\mathbf{W}_*\mathbf{A}_*)^T\{\mathbf{d}_J\} + \mu \mathbf{D}^T\mathbf{h}], \tag{8}$$

where the superscript T denotes the transposition, $\{\mathbf{d}_J\} = \{\mathbf{W}_*\mathbf{y}_* + \mathbf{W}_*\mathbf{A}_*\mathbf{m}^0\}$, $\mathbf{A}_* = \partial f_*(\mathbf{m}^0)/\partial \mathbf{m}^0$ is the combined matrix of partial derivatives for DC and TEM ($\mathbf{A}_r$ and $\mathbf{A}_t$), evaluated at an initial model $\mathbf{m}^0$, and

$$\mathbf{y}_* = \begin{bmatrix} y_r \\ y_t \end{bmatrix}$$

is the joint discrepancy vector formed by $\mathbf{y}_r = \mathbf{d}_s - gf_r(\mathbf{m}^0)$ and $\mathbf{y}_t = \mathbf{d}_t - f_t(\mathbf{m}^0)$.

The solution to (7) is (see Meju 1994, eqn 40)

$$\mathbf{M}_{q^0} = [(\mathbf{W}_*\mathbf{A}_*)^T(\mathbf{W}_*\mathbf{A}_*) + \mathbf{D}^T\mathbf{D}]^{-1}[(\mathbf{W}_*\mathbf{A}_*)^T\{\mathbf{d}_J\} + \mathbf{D}^T\mathbf{h} - \mu\mathbf{b}], \tag{9}$$

where

$$\mu = \pm(\{q_0 - q_{LS}\}/\{\mathbf{b}^T[(\mathbf{W}_*\mathbf{A}_*)^T(\mathbf{W}_*\mathbf{A}_*) + \mathbf{D}^T\mathbf{D}]^{-1}\mathbf{b}\})^{1/2},$$

and is determined by the constraint $Q_1 + Q_2 = q_0$. Thus, providing that $q_{LS} < q_0$, there are two possible solutions for μ (the so-called plus and minus solutions) which are maximally consistent with the DC and TEM field data in this adaptation of the iterative most-squares technique (see Meju 1994).

Operationally, for the initial estimate of the static-shift factor (i.e. g_a), we obtain the corresponding $\mathbf{h}$ (as either a smooth or blocky model) from a simple transform (Meju 1995, 1998) of the TEM data and normalized DC data (i.e. $\mathbf{d}_s/g_a$). We then perform an iterative search for the best-fitting least-squares model with $\chi^2 = q_{LS}$ for which we compute the measure U_2. The procedure is repeated using a simple update scheme for g and $\mathbf{h}$ and we accept the g-value that leads to the model ($\mathbf{m}$) with the smallest value of the measure U_2. The desired model ($\mathbf{m}_{q0}$) is then determined using the most-squares method (equations (7) and (9)). It is thus a combined direct and iterative joint DC-TEM inversion scheme. It is also data consistent since the models are biased towards $\mathbf{h}$ (which can admit any reliable *a priori* information). If the DC data are not affected by static shift, the inversion scheme should yield a g-value of unity. As in standard practice, the logarithmic values of the apparent-resistivity data are considered in this joint inversion scheme. The components of $\mathbf{m}$ are also taken to be the logarithms of the resistivity and depth to the base of each layer (in preference to the layer thickness) in the sought subsurface model.

The result of joint inversion of the Leicester DC sounding in the north–south direction and the central-loop TEM data for two transmitter-loop sizes (with the recording units placed outside the transmitter loops) is summarized in Fig. 6. The optimal value determined for g is 1.4815 and the final resistivity-versus-depth transformation of the field data ($\mathbf{h}$) is also shown for comparison with the joint 1D inversion model in this figure. The optimal 7-layer most-squares models (only the plus solution is shown in Fig. 6a) matched the data satisfactorily (rms error of 1). The theoretical DC and TEM responses of the most-squares plus solution are shown in Fig. 6(b), together with the actual field data and the resulting static-shift-corrected DC sounding curve from the joint inversion exercise. About 20 m of glacial deposits (sand and boulder clay) are known to overlie the Mercian Mudstone sequence at this site (R. Clements 2000, pers. comm.). The mudstone sequence may contain intercalations of marl, gypsum or anhydrite. In the joint 1D inversion model, the geoelectric units in the top 18 m (layers 1–3) correlate with the glacial cover, and the Mercia Mudstone appears to extend down to about 180 m.

Shallow seismic reflection mapped the base of this mudstone sequence at 190 m (I. Hill 2000, pers. comm.).

It is important to stress that effective joint inversion of DC resistivity and TEM data should be preceded by compatibility considerations to ascertain their dimensionality characteristics and hence the suitability of the adopted interpretational framework (i.e. whether 1D, 2D or 3D modelling is required) as is now routine practice in MT prospecting (see, e.g., Bahr 1988, 1991; Groom and Bailey 1989). For collocated DC-TEM surveys, those sites with parallel bi-directional DC and multigeometry TEM apparent-resistivity sounding curves in the log domain may be taken as being somewhat stratified, while those with significantly divergent trends would require multidimensional analysis. An illustrative case study from a complex glacial environment with borehole data (for ground truthing) is presented in the next section.

CASE STUDY OF AQUIFER CHARACTERIZATION BY JOINT INVERSION OF TEM AND DISTORTED DC DATA

Traditional discrete DC soundings were conducted in the Vale of York in northern England (Hawkins and Chadha 1990) where glacial deposits overlie the Triassic Sherwood Sandstone (SS) aquifer and Mercia Mudstone (MM) group (Fig. 7). The glacial deposits are heterogeneous and both the Mercia Mudstone and Sherwood Sandstone contain intercalations of marl, gypsum or anhydrite at the sounding sites (Hawkins and Chadha 1990) and the subsurface is hence considered macro-anisotropic (see Christensen 2000). The resistivity values derived from 1D modelling of the DC soundings by Hawkins and Chadha (1990) were anomalously high and at variance with well-log resistivities for the Sherwood Sandstone, prompting a follow-up TEM investigation of these sites by Meju, Fenning and Hawkins (2000). The data from these investigations have so far been inverted separately. The available DC and TEM soundings for six stations (PF, LH, BH, CP, GH, GS) near the boreholes, whose stratigraphic logs are listed in Table 1, may thus serve to evaluate the data analysis procedures suggested above.

The collocated DC and TEM soundings were first analysed using the suggested scaling relationships to determine the presence of any static shift in the DC data and their suitability for joint 1D inversion (see Fig. 8). Four of these DC sounding curves exhibit substantial vertical shifts relative to the overlapping TEM curves. The DC field curves also exhibit a good degree of parallelism with the TEM curves and may thus be
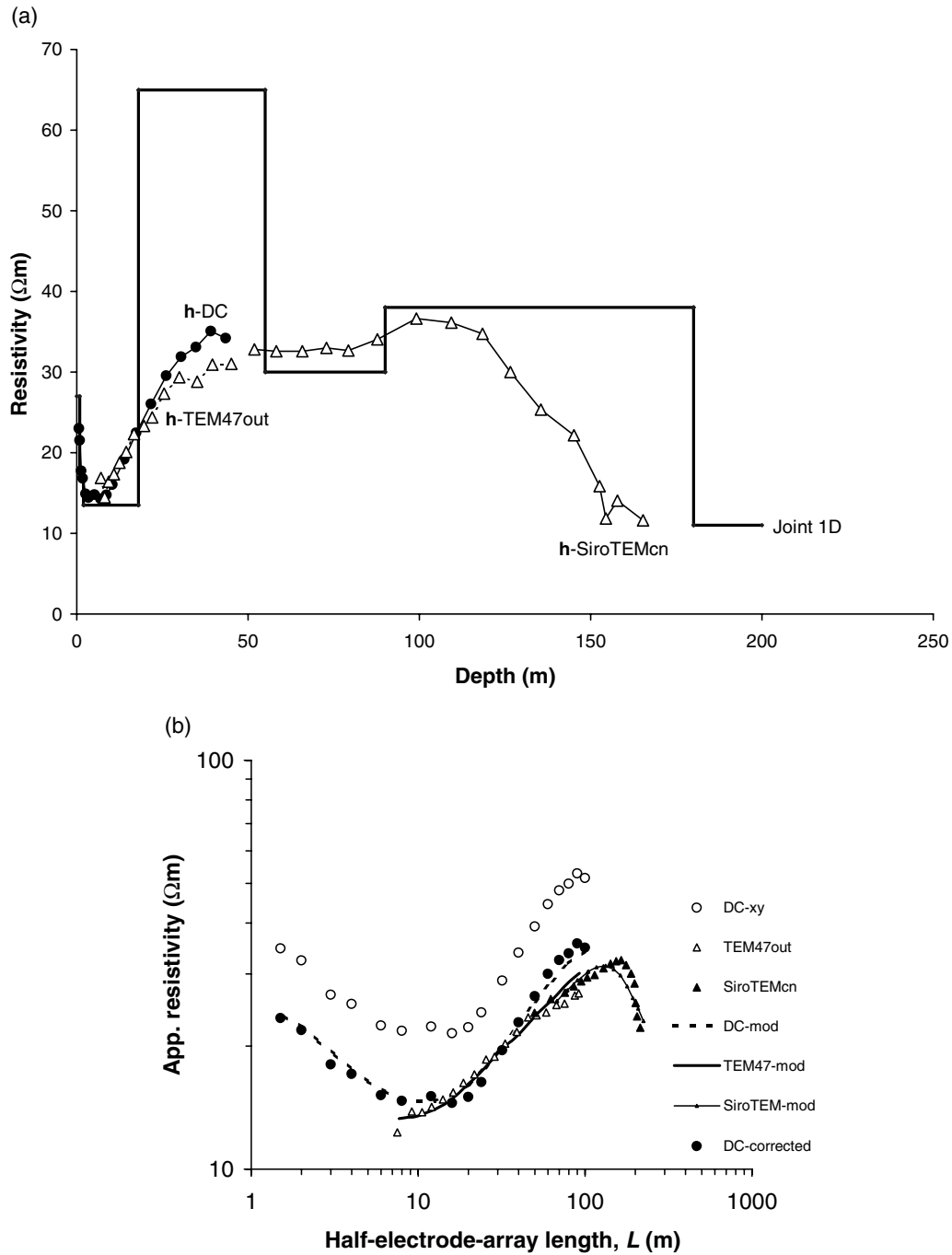
(a)

(b)

Figure 6 Summary of the result of 1D joint inversion of DC and TEM data from the Leicester test site. The north–south DC resistivity, TEM47out and SiroTEMcn data were jointly inverted. (a) The 7-layer model for the most-squares plus solution (blocky structure) and the resistivity–depth transform (**h**) of the apparent-resistivity data (Meju 1995, 1998), taking into account the determined optimal value of *g*. From top to bottom in the 1D inversion model, the layer resistivities are 27, 18, 13.5, 65, 30, 38 and 11 Ωm and the depths-to-base of the layers are 0.9, 2, 18, 55, 90 and 181 m. ●——●, **h**-DC; △–––△, **h**-TEM47out; △——△, **h**-SiroTEMcn; bold line, joint 1D. (b) The fit between field and model responses. The model responses (mod), the observed DC curve (DC-xy) and the resulting DC curve obtained from joint inversion (DC-corrected) are shown for comparison.
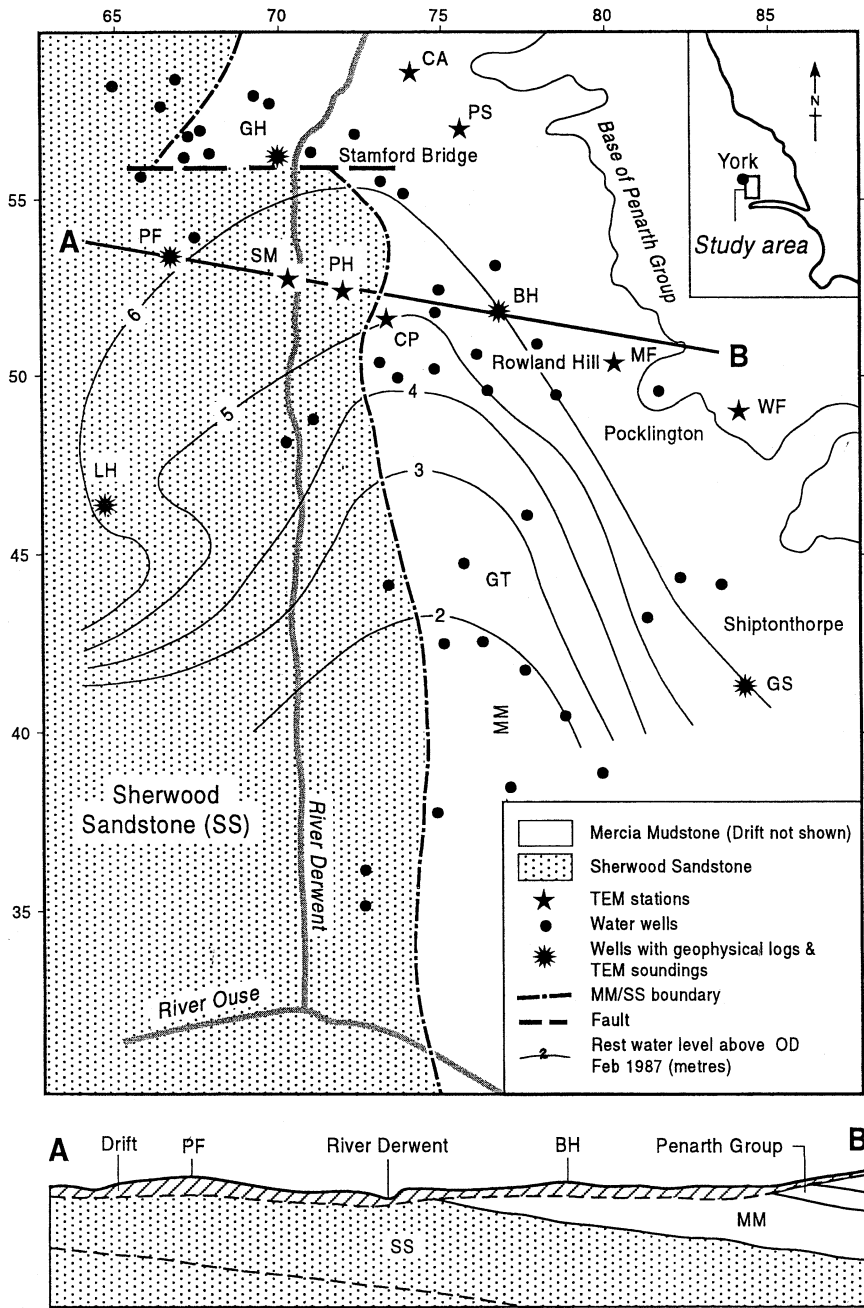
Figure 7 Location map of collocated DC resistivity and TEM soundings in the Vale of York in England (after Meju *et al.* 2000). The DC and TEM data for stations LH, PF, GH, CP, BH and GS are jointly inverted in this paper.

deemed 1D invertible (assuming that any attendant 3D galvanic distortion arises solely from small-sized surficial heterogeneities). All the data have been inverted in 1D using the algorithm described above. Since we are interested in blocky models for comparison with the available ground truth (borehole stratigraphic boundaries in Table 1) at these sites, the vector **h** is structured accordingly and held fixed at the determined optimal value of *g* until the expected misfit ($\chi^2 \approx$ number of field data). The resulting joint inversion models (Table 2) satisfactorily matched the field data shown in Fig. 8 with rms error of ≈ 1 and were derived without incorporating well-log information in **h**. Resistivity well logs are available only for

Table 1 A summary of lithological logs from various drillers for six boreholes (LH, PF, CP, GH, BH and GS) in the Vale of York study area (after Meju *et al*. 2000)

Borehole name	Lithology	Depth to base (m)
LH	Top soil	0.5
	Sand	5.0
	Boulder clay	24.5
	Sandstone with some marl bands	40.0
	Sandstone	73.0+
PF	Sandy drift	4.0
	Clayey drift	26.5
	Sandstone	77.0+
CP	Sandy drift	3.1
	Clay drift	12.0
	Mudstone	31.0
	Sandstone	70.0 +
GH	Sandy drift	3.5
	Clay drift	20.1
	Mudstone (+ beds of gypsum and anhydrite)	68.0
	Sandstone	116.0+
BH	Sandy clay drift	8.0
	Mudstone	46.0
	Marl	81.0
	Mudstone	109.0
	Sandstone	150.0+
GS	Top soil	0.5
	Sand and gravel	2.5
	Red clay with chalk gravel (till)	8.0
	Marl and mudstone	46.0
	Marl with gypsum and anhydrite beds	187.0
	Sandstone	214.0+

the uncased section of the Sherwood Sandstone aquifer for PF, GH and BH (Hawkins and Chadha 1990). They are of variable quality. The 1D joint inversion model for station PF is shown in Fig. 9 together with the well logs for comparison. The resistivity obtained by joint DC-TEM inversion for the aquiferous sections agrees with the well logs for PF and GH. The Sherwood Sandstone aquifer was not resolved at station BH (see Table 2) due to insufficient DC and TEM data.

The optimal 1D models derived for all six borehole sites, their stratigraphic correlations (as gauged from the logs given in Table 1), and the optimal estimates of static-shift parameters are summarized in Table 2. Note the good correlation between the reconstructed resistivity boundaries and the actual stratigraphic boundaries. The glacial cover is relatively

well mapped in the eastern sector of the study area (around sites BH and GS in Fig. 7), where the clay drift acts as a good marker horizon with a depth-to-base of about 8 m and resistivity of 9–11 Ωm. In the western sector (around sites GH, PF and LH in Fig. 7), the depth-to-base of the clay drift (or boulder clay) is about 20–25 m and its resistivity is in the range 15–20 Ωm. The clayey marker horizon is about 10–12 m deep and of 11–14 Ωm resistivity in the intervening zone (around site CP in Fig. 7). Another interesting observation from Table 2 is that the resistivity of the Sherwood Sandstone aquifer appears to decrease from about 40–60 Ωm at the stations in the west (PF, LH) to about 20 Ωm at GS down-dip in the east, where it is confined by thicker Mercia Mudstone and anhydritic/gypsiferous deposits. This is in accord with Hawkins and Chadha's (1990) observation, based on data from chemical analysis of water quality, that the salinity of the aquifer is higher where the Sherwood Sandstone is confined by thick Mercia Mudstone sequences than where drift alone covers it. The resistivity trend thus appears to suggest the existence in the Sherwood Sandstone aquifer of the Chebotarev sequence (see Price 1996, p. 180) – a natural zonation resulting from the chemical evolution of meteoric water, in which the groundwater becomes more saline down-dip from the outcropping or subcropping zone of recharge; however, additional DC-TEM soundings down-dip and multidimensional data inversion are required to verify this. The present results extend and refine the 1D TEM-based analysis of the resistivity characteristics of the Sherwood Sandstone aquifer and confining formations given by Meju *et al*. (2000; Table 2), which lacked DC resistivity constraints and thus suffered from the poor resolution of the top 8 m of the subsurface.

CONCLUDING REMARKS

The main tenet of this paper is that electrical and EM depth-sounding techniques can be easily compared in a consistent manner or combined to yield more complete profiling of the resistivity structure of the subsurface. It has been shown that the proposed scaling relationships can be applied in heterogeneous geological media enabling accurate identification and removal of static shift in MT and DC resistivity sounding curves. From the response pattern of the data sets obtained from multiple methods, an interpreter can determine at first glance whether the subsurface structure is characterized by simple stratification or multidimensional features, and can then select the appropriate mathematical model for interpreting the
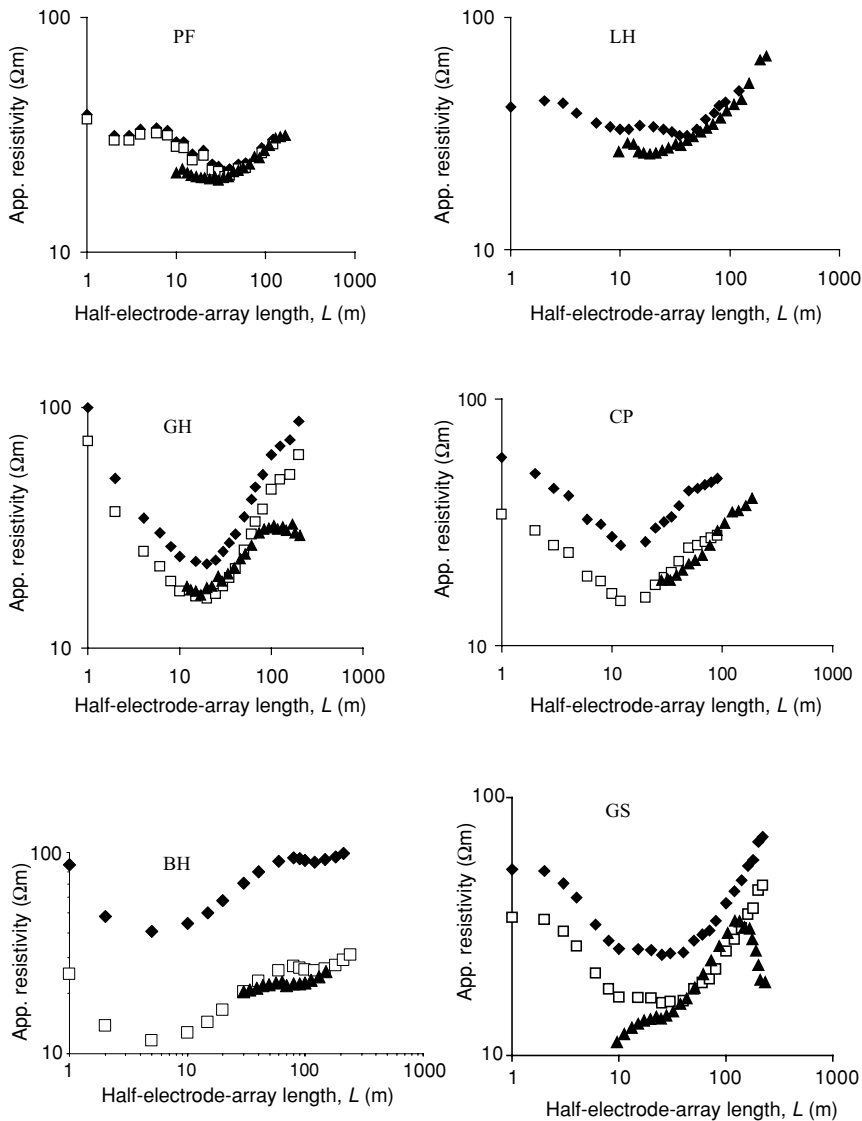
Figure 8 Comparison of DC and TEM sounding curves from six borehole sites (LH, PF, GH, CP, BH and GS) in the Vale of York. Each panel shows the observed DC data (♦) and TEM data (▲). The DC data corrected for static shift (□) that correspond to the joint inversion models presented in Table 2 are also shown.

experimental data. Electrical static shift affects the resistivity estimates in the DC (geometrical sounding) case unlike the MT (frequency sounding) situation where both the resistivity and depth estimates may be in error. A method is presented for the 1D joint inversion of TEM and distorted DC sounding data. Using the available field data sets from the Vale of York, it is shown that the method enables a good assessment of the resistivity characteristics of the Sherwood Sandstone aquifer and its confining formations. It is noted that equations (1) and (2) assume that the magnetic permeability of the subsoil is equal to that of free-space ($\mu_0 = 4\pi \times 10^{-7}$ Ωs/m), although this may not be the case over highly magnetic volcanic soils or ferrous

metal objects. Moreover, it is theoretically possible to have 'magnetic static shift' in the EM sounding curves when the heterogeneous overburden exhibits marked changes in magnetic permeability (Rijo 2003) as might occur in some volcanic terrains. In such terrains, effort should be made to obtain rock susceptibility measurements at the sounding sites to ascertain that there are no marked lateral changes in magnetic permeability before using TEM data for correcting MT or DC data. It is hoped that the simple scaling relationships given here will provide an impetus for the non-specialist to adopt integrated electrical and EM methods in routine environmental and deep geological investigations.

Table 2 Summary of the resistivity characteristics of the Sherwood Sandstone (SS) aquifer and confining formations based on the results of joint inversion of the DC-TEM soundings near six boreholes in the Vale of York study area. The averages of the two models derived from the most-squares 'plus and minus solutions' for μ in equation (9) are shown. The interpreted correlation with known lithology (Table 1) is suggested in the last column. The determined electrical static-shift factor (g) for each site is indicated against the relevant station name

| Station name/layer number	Average layer resistivity (Ωm)	Depth to base of layer (m)	Depth-correlated lithology
LH ($g = 1$)			
1	39	0.51	Top soil
2	50	1.9	Sand (dry?)
3	25	5.2	Sand (moist?)
4	46	12	Boulder clay (sandy?)
5	18.5	26.4	Boulder clay
6	60	(Not determined)	SS
PF ($g = 1.053$)			
1	43	0.5	Top soil (dry?)
2	25	1.6	Sand (partially wet?)
3	44	4.6	Sand
4	18	27	Clayey drift
5	30	70	SS (muddy section?)
6	40	(Not determined)	SS
CP ($g = 1.695$)			
1	34	0.9	Top soil
2	24	3.0	Sandy and gravel?
3	13.5	11.7	Clay drift
4	22.9	30.5	Mudstone
5	30	50.2	SS (muddy section?)
6	50	(Not determined)	SS
GH ($g = 1.39$)			
1	73	0.85	Top soil (dry?)
2	22	3.4	Sandy drift
3	14.5	22.6	Clay drift
4	98	72	Gypsiferous/anhydritic Mudstone
5	36	(Not determined)	SS
BH ($g = 3.48$)			
1	38	0.5	Top soil (?)
2	11	8.1	Clay drift
3	35	44	Mudstone
4	17	83	Marl
5	39	(Not determined)	Marl and mudstone
GS ($g = 1.54$)			
1	30	2.5	Sand and gravel
2	11	8	Till (boulder clay)
3	15	30	Marl and mudstone
4	22	45	Marl and mudstone
5	83	190	Gypsiferous/anhydritic bed
6	21	(Not determined)	SS
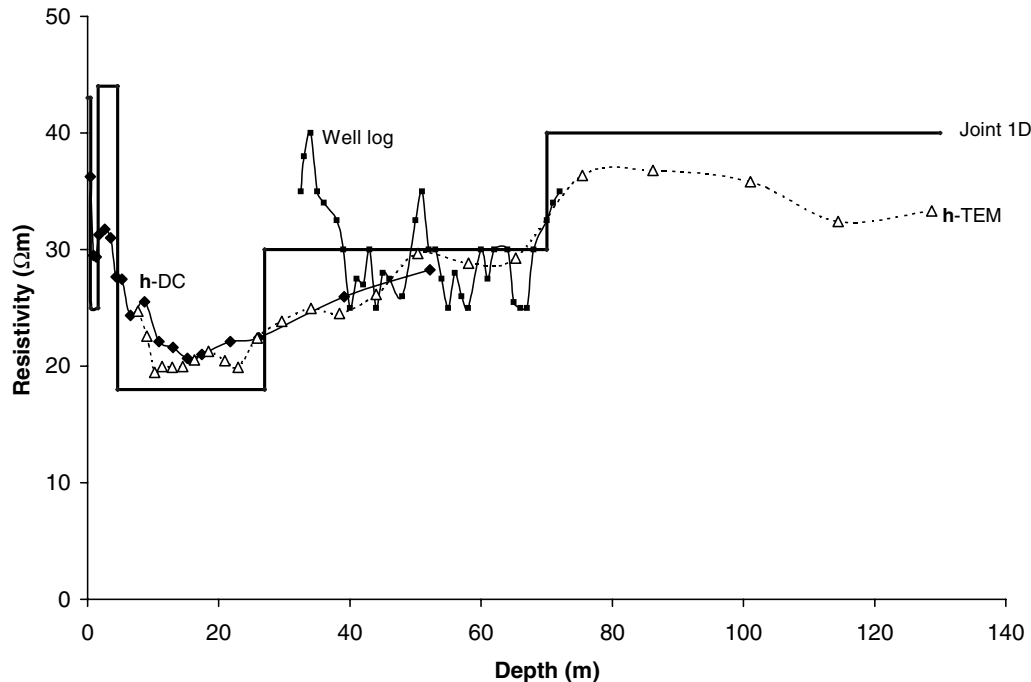
Figure 9 A comparison of the 1D joint DC-TEM inversion model and resistivity well log for station PF in the Vale of York. The 1D model (bold line) and the available resistivity log for the uncased section of SS aquifer (Hawkins and Chadha 1990, fig. 5). The direct resistivity–depth transformations (**h**) of the apparent-resistivity data (Meju 1995, 1998), taking into account the determined optimal value of *g*, are also shown. Bold line, joint 1D; ■——■, well log; △–––△, **h**-TEM; ◆——◆, **h**-DC.

REFERENCES

Auken E., Pellerin L. and Sørensen K.I. 2001. Mutually constrained inversion (MCI) of electrical and electromagnetic data. 71st SEG meeting, San Antonio, USA, Expanded Abstracts, 1455–1458 (on CD-ROM).

Bahr K. 1988. Interpretation of the magnetotelluric impedance tensor: regional induction and local telluric distortion. *Journal of Geophysics* **62**, 119–127.

Bahr K. 1991. Geological noise in magnetotelluric data: a classification of distortion types. *Physics of the Earth and Planetary Interiors* **60**, 24–38.

Bai D. and Meju M.A. 2003. Deep structure of the Longling–Ruili fault zone underneath Ruili basin near the Eastern Himalayan syntaxis: insights from magnetotelluric imaging. *Tectonophysics* **364**, 135–146.

Bai D., Meju M.A. and Liao Z. 2001. Magnetotelluric images of deep structure of the Rehai geothermal field near Tengchong, southern China. *Geophysical Journal International* **147**, 677–687.

Barker R.D. 1981. The offset system of electrical resistivity and its use with a multicore cable. *Geophysical Prospecting* **29**, 128–143.

Başokur A.T. 1994. Definition of apparent resistivity for the presentation of magnetotelluric sounding data. *Geophysical Prospecting* **42**, 141–149.

Berdichevsky M.N. and Dmitriev V.I. 1976. Distortion of magnetic and electrical fields by surface lateral inhomogeneities. *Acta Geodaetica, Geophysica et Montanista, Academy of Science of Hungary* **11**, 447–483.

Chen L., Booker J.R., Jones A.G., Wu N., Unsworth M.J., Wei W. and Tan H. 1996. Electrically conductive crust in southern Tibet from INDEPTH magnetotelluric surveying. *Science* **274**, 1694–1696.

Christensen N.B. 1995. 1D imaging of central loop transient electromagnetic soundings. *Journal of Engineering and Environmental Geophysics* **2**, 53–66.

Christensen N.B. 2000. Difficulties in determining electrical anisotropy in subsurface investigations. *Geophysical Prospecting* **48**, 1–19.

Das U.C. 1997. Multiseparation, multisystem electromagnetic depth sounding – an extension for unification. *Geophysics* **62**, 56–62.

Effersø F., Auken E. and Sørensen K.I. 1999. Inversion of band-limited TEM responses. *Geophysical Prospecting* **47**, 551–564.

Groom R.W. and Bahr K. 1992. Corrections for near surface effects: decomposition of the magnetotelluric impedance tensor and scaling corrections for regional resistivities: a tutorial. *Survey in Geophysics* **13**, 341–379.

Groom R.W. and Bailey R.C. 1989. Decomposition of the magnetotelluric impedance tensor in the presence of local three-dimensional galvanic distortion. *Journal of Geophysical Research* **94**, 1913–1925.

Habberjam G.M. and Watkins G.E. 1976. The reduction of lateral effects in resistivity probing. *Geophysical Prospecting* **15**, 221–235.

Hautot S., Tarits P., Whaler K., Le Gall B., Tiercelin J.-J. and Le Turdu C. 2000. Deep structure of the Baringo rift basin (central Kenya) from three-dimensional magnetotelluric imaging: implications for rift evolution. *Journal of Geophysical Research* **105**, 23493–23518.

Hawkins J.R.T. and Chadha D.S. 1990. Locating the Sherwood Sandstone aquifer with the aid of resistivity surveying in the Vale of York. *Quarterly Journal of Engineering Geology* **23**, 229–241.

Hobbs B.A. 1992. Terminology and symbols for use in studies of electromagnetic induction in the earth. *Surveys in Geophysics* **13**, 489–515.

Jupp D.L.B. and Vozoff K. 1977. Resolving anisotropy in layered media by joint inversion. *Geophysical Prospecting* **45**, 460–470.

Lee F.W. and Swartz J.H. 1930. *Resistivity of oil-bearing beds*. Technical Paper 488, US Bureau of Mines.

Liao Z. and Zhao P. 1999. *Yunnan–Tibet Geothermal Belt – Geothermal Resources and Case Histories*. Science Press, Beijing.

Meekes J.A.C. and van Will M.F.P. 1991. Comparison of seismic reflection and combined TEM/VES methods for hydrogeological mapping. *First Break* **9**, 543–551.

Meju M.A. 1994. Biased estimation: a simple framework for parameter estimation and uncertainty analysis with prior data. *Geophysical Journal International* **119**, 521–528.

Meju M.A. 1995. Simple effective resistivity–depth transformation for infield or real-time data processing. *Computers and Geosciences* **21**, 985–992.

Meju M.A. 1996. Joint inversion of TEM and distorted MT soundings: Some effective practical considerations. *Geophysics* **61**, 56–65.

Meju M.A. 1998. A simple method of transient electromagnetic data analysis. *Geophysics* **63**, 405–410.

Meju M.A. 2000. Geoelectrical investigation of old/abandoned landfill sites in urban areas: Model development with a genetic diagnosis approach. *Journal of Applied Geophysics* **44**, 115–150.

Meju M.A. 2002. Geoelectromagnetic exploration for natural resources: models, case studies and challenges. *Surveys in Geophysics* **23**, 133–205.

Meju M.A., Fenning P.J. and Hawkins T.R.W. 2000. Evaluation of small-loop transient electromagnetic soundings to locate the Sherwood Sandstone aquifer and confining formations at well sites in the Vale of York, England. *Journal of Applied Geophysics* **44**, 217–236.

Meju M.A., Fontes S.L., Oliveira M.F.B., Lima J.P.R., Ulugergerli E.U. and Carrasquilla A.A. 1999. Regional aquifer mapping using combined VES-TEM-AMT/EMAP methods in the semi-arid eastern margin of Parnaiba Basin, Brazil. *Geophysics* **64**, 337–356.

Meju M.A., Gallardo L.A. and Mohamed A.K. 2003. Evidence for correlation of electrical resistivity and seismic velocity in heterogeneous near-surface materials. *Geophysical Research Letters* **30**, 1373–1376.

Mohamed A.K., Meju M.A. and Fontes S.L. 2002. Deep structure of the northeastern margin of Parnaiba basin, Brazil, from magnetotelluric imaging. *Geophysical Prospecting* **50**, 589–602.

Morrison H.F., Shoham Y., Hoversten G.M. and Torres-Verdin C. 1996. Electromagnetic mapping of electrical conductivity beneath the Columbia basalts. *Geophysical Prospecting* **44**, 963–986.

Panissod C., Dabas M., Hesse A., Jolivet A., Tabbagh J. and Tabbagh A. 1998. Recent developments in shallow-depth electrical and electrostatic prospecting using mobile arrays. *Geophysics* **63**, 1542–1550.

Park S.K. 1985. Distortion of magnetotelluric sounding curves by three-dimensional structures. *Geophysics* **50**, 786–797.

Pellerin L. and Hohmann G.W. 1990. Transient electromagnetic inversion: a remedy for magnetotelluric static shift. *Geophysics* **55**, 1242–1250.

Price M. 1996. *Introducing Groundwater*, 2nd edn. Chapman & Hall.

Raiche A.P. 1984. The effect of ramp function turn-off on the TEM response of a layered ground. *Exploration Geophysics* **15**, 37–41.

Raiche A.P., Jupp D.L.P., Rutter H. and Vozoff K. 1985. The joint use of coincident loop transient electromagnetic and Schlumberger sounding to resolve layered structures. *Geophysics* **50**, 1618–1627.

Rijo L. 2003. Magnetic static shift effects on 2-D TE magnetotelluric soundings. 8th International Congress of the Brazilian Geophysical Society, Rio de Janeiro, Expanded Abstracts, 770 (on CD-ROM).

Sakkas V., Meju M.A., Khan M.A., Haak V. and Simpson F. 2002. Magnetotelluric images of the crustal structure of Chyulu Hills volcanic field, Kenya. *Tectonophysics* **346**, 169–185.

Sørensen K.I. 1996. Pulled array continuous electric profiling. *First Break* **14**, 85–90.

Sørensen K.I. 1997. The pulled array transient electromagnetic method. *Proceedings of the 3rd Meeting of EEGS-ES*, Aarhus, Denmark, pp. 135–138.

Spies B.R. 1983. Recent developments in the use of surface electrical methods for oil and gas exploration in the Soviet Union. *Geophysics* **48**, 1102–1112.

Spies B.R. and Eggers D.E. 1986. The use and misuse of apparent resistivity in electromagnetic methods. *Geophysics* **51**, 1462–1471.

Spitzer K. 2001. Magnetotelluric static shift and direct current sensitivity. *Geophysical Journal International* **144**, 289–299.

Sternberg B.K., Washburne J.C. and Pellerin L. 1988. Correction for the static shift in magnetotellurics using transient electromagnetic soundings. *Geophysics* **53**, 1459–1468.